1 Protein features for assembly of the RNA editing helicase 2 subcomplex (REH2C) in
2 Trypanosome holo-editosomes

3

4 Vikas Kumar[1#], Pawan K. Doharey[1#], Shelly Gulati[2#], Joshua Meehan[1], Mary G. Martinez[1],
5 Karrisa Hughes[2], Blaine H.M. Mooers[2*] and Jorge Cruz-Reyes[1*]

6

7 [1] Department of Biochemistry and Biophysics, Texas A&M University, College Station, Texas,
8 United States of America.

9 [2] Department of Biochemistry & Molecular Biology, University of Oklahoma Health Sciences
10 Center, Oklahoma City, Oklahoma, United States of America.

11

12 * Corresponding author:

13 e-mail: cruzrey@tamu.edu

14 * Correspondence may also be addressed to:

15 e-mail: blaine-mooers@ouhsc.edu

16

17 # These authors contributed equally to this work.

18

19

Abstract

Uridylate insertion/deletion RNA editing in *Trypanosoma brucei* is a complex system that is not found in humans, so there is interest in targeting this system for drug development. This systeme uses hundreds of small non-coding guide RNAs (gRNAs) to modify the mitochondrial mRNA transcriptome. This process occurs in holo-editosomes that assemble several macromolecular *trans* factors around mRNA: the RNA-free RNA editing core complex (RECC) and auxiliary RNPs. Yet, the regulatory mechanisms of editing remain obscure. The enzymatic accessory RNP complex, termed the REH2C, includes mRNA substrates and products, the multi-domain 240 kDa RNA Editing Helicase 2 (REH2) and an intriguing 8-zinc finger protein termed REH2-Associated Factor 1 (^{H2}F1). Both proteins are essential in editing. REH2 is a member of the DExH/RHA subfamily of RNA helicases with a conserved C-terminus that includes a regulatory OB-fold domain. In trypanosomes, ^{H2}F1 recruits REH2 to the editing apparatus, and ^{H2}F1 downregulation causes REH2 fragmentation. Our systematic mutagenesis dissected determinants in REH2 and ^{H2}F1 for the assembly of REH2C, the stability of REH2, and the RNA-mediated association of REH2C with other editing *trans* factors. We identified functional OB-fold amino acids in eukaryotic DExH/RHA helicases that are conserved in REH2 and impact the assembly and interactions of REH2C. ^{H2}F1 upregulation stabilized the large REH2 polypeptide *in vivo*. Mutation of the core cysteines or basic amino acids in individual zinc fingers affected the stabilizing property of ^{H2}F1 but not its interactions with other examined editing components. Thus, most if not all fingers may contribute to REH2 stabilization. Finally, a recombinant REH2 (240 kDa) established that the full-length protein is a *bona fide* RNA helicase with ATP-dependent unwinding activity. REH2 is the only DExH/RHA-type helicase in kinetoplastid holo-editosomes.

45

46 # Introduction

47

48 Kinetoplastid protozoa including *Trypanosoma brucei* are early-branching eukaryotes
49 that require extensive insertion and deletion of uridylates in most mitochondrial mRNAs
50 (reviewed in 1). This RNA editing is protein-catalyzed and directed by small guide RNAs
51 (gRNAs) that exhibit complementarity to fully edited mRNA via Watson-Crick and wobble G•U
52 base pairs. Most editing progresses in blocks that typically overlap and each block is directed by
53 a single gRNA (2). The editing machinery includes multiple subcomplexes: the ~20S catalytic
54 RNA editing core complex (RECC, also called the 20S editosome) and auxiliary editing RNPs.
55 The ~15S REH2-associated complex (REH2C) characterized here includes RNA editing
56 helicase 2 (REH2), REH2-associated protein factor 1 (^{H2}F1), ^{H2}F2, and mRNA substrates and
57 products (3, 4). However, only REH2 and ^{H2}F1 participate in editing. REH2C interacts physically
58 and functionally with a larger accessory editing RNP complex termed the RNA editing substrate
59 binding complex (RESC), which also contains mRNA substrates and products (5, 6). The
60 presence of mRNA in RESC was confirmed by others (7, 8). RESC contains two modules that
61 are intimately associated with each other: the gRNA-binding complex (GRBC) typified by the
62 GAP1/GAP2 (alias GRBC2/GRBC1) heterotetramer that binds and stabilizes gRNA, and the
63 more loosely defined RNA editing mediator complex (REMC) typified by RGG2 (6). REMC
64 includes proteins that promote editing progression (8-10). Other mRNA *trans* factors include a
65 subcomplex containing MRB6070 and MRB1590, and RNA helicase REH1 that associate with
66 holo-editosomes via stable or transient RNA contacts, respectively (11-13). The editing
67 apparatus is further complicated by the occurrence of variants of GRBC, REMC and RECC
68 (reviewed in 1). The dynamic nature of the holo-editosome may be relevant in editing control
69 and is reminiscent of the intricate molecular dynamics of the RNP complexes involved in mRNA
70 splicing and transcription.

71

72 The finding that the editing RNPs described above carry mRNA and gRNA implied that
73 mRNA-gRNA hybrids form on multi-RNP platforms, and that transient addition of the RECC
74 enzyme to the substrate-loaded platforms completes the assembly of the holo-editosome (3-8).
75 The precise control mechanisms in editing remain unclear. However, the helicase REH2C
76 subcomplex may play an important regulatory role. REH2 is the largest characterized member
77 of the DExH/RNA helicase A (RHA) subfamily of proteins (14). These proteins are monomeric
78 and contain a conserved C-terminal domain cluster that includes the characteristic auxiliary
79 oligonucleotide-binding (OB fold) domain (3, 14-16). The OB fold in some RNA helicases is
80 known to bind protein regulators or mediate RNA-dependent activation of these enzymes (17).
81 DExH/RHA proteins have a N-terminus with a variable domain organization of less clear
82 function. The N-terminal half of the REH2 carries two predicted double-stranded RNA binding
83 domains: dsRBD1 and dsRBD2 (14). Other characterized DExH/RHA-type proteins that carry
84 two N-terminal dsRBDs are the RNA helicase RHA (aka DHX9) in vertebrates and its
85 orthologous RNA helicase MLE (*maleless*) in flies (18). Recombinant versions of the REH2 N-
86 terminal half and full-size octa-zinc finger ^{H2}F1 formed a stable complex *in vitro* (4). However,
87 ^{H2}F1 is an unusual binding partner of DExH/RHA proteins that typically associate with G-patch
88 proteins (17). A genetic knockdown of ^{H2}F1 prevented RNA-mediated association of REH2 with
89 other editing components and caused fragmentation of REH2 *in vivo*, so ^{H2}F1 serves as an
90 adaptor protein and may stabilize REH2 (4).

91 The current study identified features in REH2 and ^{H2}F1 that affect the binding of these
92 proteins with each other, the stability of REH2, and RNA-mediated stable or transient
93 association of the REH2C subcomplex with other editing components *in vivo*. About 20 different
94 protein variants were examined *in vivo*. Comparisons of the REH2 with other eukaryotic
95 DExH/RHA helicases identified conserved OB fold residues that affect the assembly and

interactions of REH2C and are also important in distant processes, namely mRNA splicing in yeast, and the assembly of the dosage compensation complex in fly. ^{H2}F1 upregulation stabilized the large REH2 polypeptide *in vivo*. However, mutation of individual zinc fingers compromised the stabilizing property of ^{H2}F1 but not its association with REH2 or other examined components of the editing apparatus. Thus, most if not all fingers may contribute to REH2 stabilization. Finally, we used a recombinant protein construct to establish that the isolated full-length REH2 (240 kDa) is a *bona fide* RNA helicase enzyme with ATP-dependent unwinding activity. REH2C is most likely an enzymatic editing RNP in kinetoplastid holo-editosomes.

Results

Previous studies revealed that the native REH2C exhibits RNA-mediated interactions with at least two variants of RESC (3-5). These variants contain gRNA and comparable levels of GAP1 and RGG2, that typify GRBC and REMC, respectively. However, these variants differ minimally in their relative content of the canonical MRB3010 in GRBC. Additional variations in protein composition have been reported in purifications of RESC components by different labs (reviewed in 1). Interestingly, native and genetically-induced changes in MRB3010 stoichiometry may be common. While the precise reasons of these changes are unclear, we reasoned that they reflect relevant dynamic changes in the assembly and function of the editing apparatus. In this study, we examined protein features that affect the formation of REH2C, its stable association with RESC components, and transient contacts with the RECC enzyme. Because the examined helicase-associated RESC variant exhibits substoichiometric MRB3010, we refer to its variant GRBC module as GRBC* (4). We have detected other proteins in this RESC

120 variant using antibodies made available to us, including: MRB8170 and MRB6070 (data not
121 shown). However, further analysis of relative composition between variants is needed.
122

123 Analysis of REH2 mutants *in vivo*
124
125 We analyzed the importance of specific features of REH2, both in the formation of REH2C
126 and in the association of this subcomplex with other components in holo-editosomes (constructs
127 listed in Fig. 1A). To this end, we expressed a tetracycline-inducible tagged REH2 wild-type (WT)
128 construct and examined its co-purification with endogenous ^{H2}F1 and GAP1 proteins, in the REH2C
129 and GRBC, respectively. We found that ectopic REH2 was able to reconstitute interactions of the
130 native REH2 protein in trypanosomes (Fig. 1B-C, lanes 1-2, respectively). With this system in hand,
131 we began testing the assembly of REH2 variants bearing truncations or point mutations in an
132 approach that has been used in other eukaryotic DExH/RHA helicases (16, 19). Neither
133 overexpression or depletion of REH2 affects the steady-state level of its binding partner ^{H2}F1 or
134 the examined GRBC proteins (3, 4).
135

136 **Fig. 1. *In vivo* analyses of REH2 variants. (A)** Scheme of REH2 WT (2167 residues) and
137 variants with the examined truncations or point mutations in the N- and C-terminal regions (NTR
138 and CTR). The mutations, affected domains, and predicted molecular weight of the constructs
139 are listed. Identified domains: dsRBD1 and dsRBD2 (double-stranded RNA binding domains 1
140 and 2), CORE (catalytic core RecA1 and RecA2 domains), HA2 (helicase associated helical
141 bundle domain), and OB (OB fold-like domain). **(B-C)** Western blots of IgG pulldowns from
142 extracts to examine the association of tagged REH2 WT or deletion mutants with endogenous
143 ^{H2}F1 and GAP1. An uninduced (-Tet) control lane is included. The GAP1 panels derive from
144 equivalent pulldowns with the same recovery of tagged protein (data not shown). The data are
145 representative of at least three biological replicates for each mutant. A few non-specific species

146 cross-react with the antibodies in some assays. The position of IgG is marked. Sizing markers
147 (M) are in kDa. **(D)** Charts of the relative level of ^{H2}F1 and GAP1 in the pulldowns.
148 Representative assays from panels A-B and other pulldowns in this study were used to plot +/-1
149 SD, *n*=3 for each mutant. The ^{H2}F1/REH2 and GAP1/REH2 ratios in each REH2 mutant were
150 normalized to the ratios in REH2 WT (= 1, in the plot). Assays with signals that too low were not
151 measured (not determined, n.d.). REH2 was often fragmented, so only the full-length
152 polypeptide was scored. Some short variants were present at higher level than REH2 WT in the
153 induced extracts.
154
155 *N- and C-truncations*. We examined N- and C-terminal regions (NTR and CTR) flanking the
156 catalytic and helicase associated domains RecA1/RecA2 and HA2, respectively, in REH2. We
157 removed sequences in the unique NTR (>1000 residues) in the REH2 variants ΔN and ΔNds, or in
158 the CTR after the OB fold (123 residues) or from the OB fold (260 residues) in the ΔAOB and ΔOB
159 variants, respectively. REH2 and its orthologs in kinetoplastids are the largest known DExH/RHA-
160 type helicases and carry the longest helicase-specific N terminus (~1300 residues in REH2 from *T.*
161 *brucei*) (14). Direct comparisons with the REH2 WT construct showed that the examined N- and C-
162 resections reduced the association of the shortened REH2 polypeptides with ^{H2}F1 and GAP1 proteins
163 (Figs. 1B-D). This suggested that both termini of REH2 may contribute to the normal assembly of
164 REH2C and its RNA-mediated interactions with other editing components *in vivo*. Motifs in the
165 dsRBDs, the OB fold, and undefined features in the N and C termini may be involved. It is also
166 conceivable that the examined sequence resections impact the global conformation of REH2, thereby
167 indirectly affecting its protein interactions. Thus, the normal REH2 interactions in the editing
168 apparatus may be sensitive to overall changes in the integrity or conformation of REH2. Because the
169 CTR includes a potentially regulatory OB fold in DExH/RHA-type RNA helicases (16), we focused on
170 this domain in the subsequent studies of REH2.

171

172 *Point mutations*. Our structural searches of the OB fold-like domain in REH2 using Phyre2
173 (20) found the best agreements with reported structures of yeast ADP-bound Prp43p helicase and
174 *Drosophila* RNA helicase MLE RNA ADP Alf4 complex (4, 16, 18)(and data not shown). Prp43p is a
175 bi-functional helicase in mRNA splicing and ribosome biogenesis (15, 21). The helicase MLE
176 remodels roX RNA substrates to promote assembly of the dosage compensation complex in
177 *Drosophila* (18). We examined specific residues in the predicted OB fold of REH2 that seem to be
178 conserved in reported DExH/RHA helicase structures (Fig. 2 A-D). OB point mutations were
179 compared to two controls: REH2 WT and a reported mutation in dsRBD2 (dsR) that reduces the
180 association of REH2 with GAP1, gRNA and mRNA (Fig. 2A, lanes 1 and 2, respectively) (3). The
181 $\beta1-\beta2$ and $\beta4-\beta5$ loops in the OB fold may include determinants in nucleic acid recognition (Fig. 2D)
182 (16, 18). In helicase Prp43p, mutation of R664 or K704, which are exposed in the Prp43p structure,
183 decreased the RNA affinity and ATPase activity of the helicase *in vitro* (16). Sequence alignments
184 and a homology model using Prp43p as the template matched R664 and K704 in Prp43p with R1979
185 and R2023 in REH2, respectively (data not shown). Pulldowns of the R1979A and R2023A mutants
186 suggest that neither mutation alters the association of REH2 with ^{H2}F1 (Figs. 2A-C; and data not
187 shown). R1979A did not appear to affect the REH2 association with GAP1. However, R2023A
188 caused a moderate decrease in the association with GAP1, implying that at least R2023A could be
189 disruptive in trypanosomes. In helicase MLE, a few identified residues in the OB fold bind specific
190 uridylates in U-rich sequences in roX transcripts, and mutation of some of these residues impaired
191 RNA binding by MLE *in vitro* or the proper localization of MLE in chromosomes (18). Sequence
192 alignments and homology models indicated that the residues H1032 and K1033 in MLE likely
193 represent residues H1998 and R1999 in the $\beta3-\beta4$ loop in the OB fold in REH2 (Fig. 2D; S1 Fig; and
194 data not shown). The H1998E mutant appeared to retain a normal association with ^{H2}F1 but exhibited
195 a moderate decrease in association with GAP1. In contrast, R1999E either alone or together with

196 H1998E (98/99) exhibited a more robust decrease (over 60%) in association with both ^{H2}F1 and
197 GAP1 (Fig. 2A-C). This indicated that H1998 and R1999 contribute to the assembly of the REH2
198 helicase with other editing components. However, R1999 has a higher impact on such interactions
199 than the adjoining H1998. As expected, the dsR mutant used as a control exhibited a strong
200 decrease in association with GAP1. However, the dsR mutation did not seem to affect the
201 association of REH2 with ^{H2}F1 (Figs. 2A, 2C). Pulldowns of the mutants were normalized to the
202 REH2 WT control.
203
204 **Fig. 2. *In vivo* analyses of REH2 variants. (A)** Western blots of IgG pulldowns as in Fig. 1 to
205 examine the association of endogenous ^{H2}F1 and GAP1 with tagged REH2 WT or variants with
206 point mutations in the OB fold domain: single at R1979A (1979), H1998E (1998) and R1999E
207 (1999), or double at 1998/1999 (98/99). The previously characterized dsR mutant with an
208 inactivating double mutation in the dsRBD2 was included for comparison (3). The GAP1 panels
209 in Figs. 2A-B derived from identical pulldowns with the same recovery of tagged protein (data
210 not shown). A few non-specific species crossreact with the antibodies in some assays. **(C)**
211 Charts of the relative levels of ^{H2}F1 and GAP1 in the pulldowns. Assays from panels A-B and
212 biological replicate pulldowns in this study were used to plot +/-1 SD, *n*=2 or *n*=3 for each
213 mutant. The ^{H2}F1/REH2 and GAP1/REH2 ratios in each REH2 mutant were normalized to the
214 ratios in REH2 WT (= 1, in the plot). **(D)** Secondary structure prediction of the OB fold with α-
215 helix (cylinders) and β-strand (arrows) elements, and the position of point mutations examined
216 indicated by arrows.
217
218 Together, our systematic mutagenesis of REH2 suggests an intricate interaction network
219 including features across both N- and C- terminal regions of REH2 that affect the assembly of
220 REH2C, and the association of this subcomplex with other components of the editing apparatus *in*

221 *vivo*. Remarkably, these observations also indicate that equivalent residues in the auxiliary
222 conserved OB fold domain in DExH/RHA helicases function in disparate RNA processes in
223 taxonomically distant species of trypanosomes, yeast, and fly. While large protein truncations in
224 REH2 may alter the global conformation of the polypeptide, relevant point mutations in REH2 are
225 more likely to cause specific functional effects. Table 1 summarizes observed effects of the examined
226 mutations in REH2 on its association with ^{H2}F1 and GAP1.

227 **Table 1. Association of REH2 constructs with ^{H2}F1 and GAP1**

REH2-TAP variant	Association in pulldown		Reference
	^{H2}F1	GAP1	Construct described
WT	control*	control*	Hernandez et al. 2010
ΔN	decreased	decreased	This study
ΔNds	decreased	decreased	This study
ΔOB	decreased	decreased	This study
ΔAOB	decreased	decreased	This study
dsR	control-like †	decreased	Madina et al. 2016
1979	control-like	control-like	This study
1998	control-like	decreased	This study
1999	decreased	decreased	This study
98/99	decreased	decreased	This study
2023	control-like	decreased	This study

* The WT construct served as positive control to assess relative association of mutant constructs.

228 † Comparable to the level observed with the WT construct.
229

230 Analysis of ^{H2}F1 mutants *in vivo*

231
232 To analyze specific features of the ^{H2}F1 zinc finger protein in trypanosomes, we expressed a
233 tagged ^{H2}F1 WT construct and examined its association with endogenous REH2, GAP1 and REL1
234 proteins. We found that the tagged ^{H2}F1 WT was able to reconstitute interactions of the native ^{H2}F1
235 protein in trypanosomes (Fig. 3). Notably, expression of the ectopic ^{H2}F1 WT increased the steady-
236 state level of endogenous REH2 compared to a control lane without tetracycline (Fig. 3A, lanes 1-2;
237 Fig. 3B). As a control to mark the position of REH2 we used a reported RNAi-based knockdown of
238 ^{H2}F1 that decreases the level of endogenous REH2 (Fig. 3A, lanes 5-7; Fig. 3B)(4). The contrasting
239 effects of the upregulation and downregulation of ^{H2}F1 on the endogenous REH2 are consistent with

240 the idea that ^{H2}F1 stabilizes REH2 *in vivo*. These effects by ^{H2}F1 also imply that the interaction
241 between REH2 and ^{H2}F1 may vary *in vivo* or that these proteins are not always associated. We
242 examined canonical proteins in REH2C, RESC and RECC in sedimentation analyses of
243 mitochondrial extract (S2 Fig). REH2 is heterodispersed as shown before (22) and overlaps with ^{H2}F1
244 in the gradient. However, the relative abundance of these proteins at low and high densities differs
245 substantially. It is indeed possible that the association between REH2 and ^{H2}F1 or their stoichiometry
246 in REH2C varies *in vivo*. Additional studies will be necessary to examine these possibilities.
247
248 **Fig 3. Effect of expressing ^{H2}F1 WT or a variant lacking Znf5 (core residues C2>A2) on**
249 **the REH2 steady state. (A)** Western blots of extracts with tagged ^{H2}F1 WT (lanes 1-2) or Znf5
250 mutant (Z5; lanes 3-4). Control assays include lanes without Tet-induction. Also, control lanes
251 with a reported ^{H2}F1-RNAi construct mark the position of the endogenous REH2 and ^{H2}F1. The
252 RNAi lanes show the induced decrease of ^{H2}F1 and concurrent fragmentation of REH2 full-
253 length (4). The level of endogenous REH2 was examined. GAP1 was used as a loading control
254 in all assays in this panel. Molecular size markers (M). A typical C2H2 zinc finger domain fold is
255 depicted with core cysteine substitutions C2>A2 (arrows), other conserved residues, and
256 variable residues (black circles). **(B)** Charts of the relative levels of endogenous REH2 full-
257 length in the extracts +/-1 SD, *n*=3. Induced/uninduced ratios of REH2 for each construct were
258 further normalized to GAP1. **(C-D)** IgG pulldowns of WT and Z5 constructs showing association
259 with endogenous REH2, GAP1, REL1, and endogenous ^{H2}F1. Non-specific species (*) may
260 represent fragments of the tagged protein that react with the antibodies. **(E)** Charts of the
261 relative levels of REH2, GAP1 and REL1 in the pulldowns +/-1 SD, *n*=3. The ratios
262 (protein/tagged-bait) in the Z5 mutant were normalized to ratios in the ^{H2}F1 WT construct.
263
264 To determine if the stabilizing effect of ^{H2}F1 requires one or more zinc finger (Znf) domains,
265 we introduced amino acid substitutions that either disrupt the canonical fold of the domain (by

266 replacing the canonical residues) or eliminate the positive charge (by replacing various basic
267 residues with neutral residues) in individual fingers of the ectopic construct. The examined ^{H2}F1
268 mutants are summarized in Table 2.

269 **Table 2. ^{H2}F1 mutants with reduced ability to stabilize REH2 *in vivo***

^{H2}F1-TAP variant	Endogenous REH2 *Steady-state level*	Reference Construct described
WT	Increased*	This study
ZnF1 +>A	no change†	This study
ZnF2 +>A	no change	This study
ZnF3 +>A	no change	This study
ZnF4 +>A	no change	This study
ZnF5 +>A	no change	This study
ZnF5 C2>A2	no change	This study
ZnF1-8 C2>A2&	no change	This study
ZnF6-8 C2>A2&	no change	This study
ZnF1-4 C2>A2&	no change	This study
ΔN	no change	This study
ΔC	no change	This study

* ^{H2}F1-WT ectopic expression increased the level of endogenous REH2
† No change (i.e., level within stardard deviation of at least two biological replicates)
& Not shown. Ectopic expression was unstable or eventually lost in culture.

270
271
272 *Canonical cysteine residues*. We changed two cysteines to two alanines (C2>A2) to disrupt
273 the native conformation of the predicted zinc fingers (Fig. 3A). We began by disrupting Znf5 because
274 of its significant homology to a reported dsRNA-bound C2H2 zinc finger domain structure (4, 14, 23).
275 The resulting mutant protein (^{H2}F1 minus Znf5) did not induce an evident increase in the steady-state
276 level of endogenous REH2 as the WT ^{H2}F1. This was evident in direct comparisons of extracts that
277 contain similar levels of ectopic ^{H2}F1 protein, WT or Znf5-less (Fig. 3A, lanes 1-4; Fig. 3B). This
278 differential effect between the ^{H2}F1 WT and Znf5-less variants was similarly observed in cultures 1 or
279 3 days after induction (data not shown). So, the stabilizing property of ^{H2}F1 is independent of the
280 period of induction *in vivo*. To examine whether the lack of Znf5 affected the association of ^{H2}F1 with
281 other editing components, we performed IgG pulldown assays of tagged ^{H2}F1. These assays showed
282 that the ^{H2}F1 WT and Znf5-less variants similarly associated with endogenous helicase REH2, GAP1

283 and REL1 ligase (Figs. 3C, 3E). Notably, pulldowns of both tagged ^{H2}F1 WT and Znf5-less, contain
284 endogenous ^{H2}F1 (Fig. 3D). Thus, Znf5 is not essential for the normal association of ^{H2}F1 with other
285 editing components.

286 We also tested a ^{H2}F1 variant bearing a triple C2>A2 substitution in Znf6, Znf7 and Znf8. The
287 ^{H2}F1 triple mutant failed to stabilize endogenous REH2 but it was able to bind REH2 and GAP1 as
288 we observed with both ^{H2}F1 WT and Znf5-less constructs (data not shown). Expression of this
289 construct was unstable and eventually lost in culture (data not shown). These observations suggest
290 that ^{H2}F1 may require a full complement of zinc fingers in their native conformation to stabilize REH2
291 but not to associate with the examined editing components.

292

293 *Variable basic residues*. Because the native conformation of the zinc fingers seems to be
294 required for ^{H2}F1 to stabilize REH2 we introduced mutations to decrease the positive charge in the
295 zinc fingers. Yet these mutated fingers are likely to retain their native conformation (24). We
296 expressed ^{H2}F1 variants to test the role of several basic residues around the core residues that are
297 mostly located between the second cysteine and the first histidine (Fig. 4A) (25). Specifically, we
298 introduced R/K>A substitutions to decrease the positive charge in the zinc fingers and to remove
299 potential charge-charge interactions with REH2 or associated RNAs. Our functional analyses of Znf1,
300 Znf2, Znf3 or Zn5 showed that the loss of positive charge in any of these zinc fingers reduced the
301 ability of ^{H2}F1 to induce the accumulation of intact endogenous REH2 in extracts (Figs. 4B-C).
302 However, these mutations did not prevent the association of ^{H2}F1 with REH2, GAP1 and REL1 (Figs.
303 4D, 4F). These expressed ^{H2}F1 variants also co-purified with endogenous ^{H2}F1 at a level comparable
304 to the WT construct (Figs. 4D-F). So, the wildtype and R/K>A variant proteins associated similarly
305 with the examined editing components. Overall, ^{H2}F1 may require that most zinc fingers retain their
306 native conformation and positive charge to efficiently increase the stability of REH2. However, the
307 loss of the native conformation or positive charge in individual fingers does not preclude the
308 assembly of ^{H2}F1 in the REH2C, or the association of this subcomplex with the examined editing

309 components. Detection of endogenous ^{H2}F1 in our pulldowns suggest the presence of ^{H2}F1
310 multimers. Pulldowns treated with an RNaseA/T1 mixture suggest that the association between
311 tagged ^{H2}F1 and endogenous ^{H2}F1 is RNase-resistant (S3 Fig.). However, further studies using
312 isolated recombinant proteins are needed to establish direct protein contacts between ^{H2}F1
313 monomers as it was shown between REH2 and ^{H2}F1 (4).
314
315 **Fig. 4. *In vivo* analyses of ^{H2}F1 variants with reduced positive charge in Znf1, Znf2, Znf3**
316 **or Znf5 (variable residues R/K>A). (A)** Cartoon of ^{H2}F1 (524 residues). Multi-sequence
317 alignment of the eight C2H2 zinc fingers, indicating the core cysteines and histidines (boxes)
318 and variable basic residues in each finger (open circles). Depiction of a C2H2 zinc finger
319 domain fold, and variable residue substitutions R/K>A. **(B)** Extracts as in Fig. 3A of induced
320 tagged ^{H2}F1 WT and Z1, Z2, Z3 and Z5 mutants or uninduced control. GAP1 was used as a
321 loading control (lanes 1-7). **(C)** Chart of steady-state level of endogenous REH2 full-length in
322 extracts with each construct as in Fig. 3B. **(D-E)** IgG pulldowns of ^{H2}F1 WT and Z1, Z2, Z3 and
323 Z5 mutants showing association with endogenous REH2, ^{H2}F1, REL1 and GAP1. Non-specific
324 species in pulldowns (*) are indicated. (**F)** Charts of the relative levels of associated
325 endogenous proteins in the pulldowns +/-1 SD, *n=2* or *n*=3, as in Fig. 3.
326
327 *N- and C-truncations*. Because mutagenesis of the tested Znf domains did not prevent the
328 association of ^{H2}F1 with other editing components *in vivo*, we asked if fragments of ^{H2}F1 retain these
329 interactions. To test this question, we expressed N- or C-terminal fragments including Znf1-to-Znf3
330 (termed ∆C) or Znf4-to-Znf8 (termed ∆N) that span 49% and 51% of the ^{H2}F1 polypeptide chain,
331 respectively (Fig. 5A, bottom). These two fragments exhibited minimal or no association with the
332 examined endogenous REH2, ^{H2}F1, or REL1 ligase (Figs. 5A). Independent pulldowns of the ^{H2}F1
333 truncated constructs confirmed these defects in association (data not shown). These mutants were
334 directly compared with the ^{H2}F1 WT and Znf4 (R/K>Ala) constructs. The Znf4 like other Znf mutations

335 in the current study retained all tested interactions that are observed with the ^{H2}F1 WT control. Thus,
336 the ΔN and ΔC constructs failed to establish basic interactions with the tested editing components.
337 Because the native REH2C subcomplex carries mRNA (4), we wondered if the ^{H2}F1 ΔN and ΔC
338 constructs also fail to co-purify with mRNA. To this end, we quantitated the relative content of
339 mitochondrial transcripts in the pulldowns of the WT, ΔN, and ΔC constructs in biological replicate
340 experiments that were performed in triplicate (Fig. 5B). The examined mitochondrial transcripts
341 include examples of unedited, edited, and never-edited mRNA, the never-edited mRNA ND4, and
342 ribosomal RNA 9S. We also examined cytosolic transcripts (Tubulin, 1400 and 1390) to score non-
343 specific RNA interactions of editing subcomplexes as in previous pulldown studies (5). Relative to the
344 ^{H2}F1 WT control used for normalization, both ΔN and ΔC pulldowns exhibited a dramatic loss in
345 bound mitochondrial mRNAs (Fig. 5B, upper and middle panels). Interestingly, the levels of cytosolic
346 mRNAs were similar in the ΔN and WT proteins but dramatically less in the ΔC variant. We also
347 compared the relative impact of the ΔN and ΔC deletions with a more discrete alteration in the Znf4
348 construct (R/K>Ala); Fig. 5B, lower panel). The level of mitochondrial RNAs in the Znf4 pulldown was
349 similar to that of the ^{H2}F1 WT control. However, the level of cytosolic transcripts decreased ~70 fold
350 in Znf4. The independent pulldowns and RNA quantitation in three equivalent experiments showed
351 consistent results in the protein interactions and RNA content of these ^{H2}F1 constructs. (Fig. 5A).
352 Thus, the tested ^{H2}F1 fragments appear to have lost the normal direct interaction of ^{H2}F1 WT with
353 REH2 in REH2C and the RNA-dependent association of ^{H2}F1 WT with other examined proteins in the
354 editing apparatus. Quantitation of the examined transcripts in the input extracts (including those used
355 in the pulldowns in Figs. 5A-B) confirmed that the observed dramatic loss in RNA association with ΔN
356 and ΔC constructs was not due to large changes in the transcripts levels at steady state (S4 Fig.).
357 The above observations indicated that features in both termini of ^{H2}F1 are required for efficient
358 association of mitochondrial transcripts in the pulldowns of ^{H2}F1. Also, C-terminal features in ^{H2}F1
359 potentially including Znf4-to-Znf8, may be largely responsible for the observed non-specific

360 association of cytosolic transcripts in the pulldowns of ^{H2}F1 (Fig. 5B, compare the top and middle
361 panels). Finally, the more discrete mutation in Znf4 may have caused a relatively mild decrease in
362 RNA affinity that mostly affected weak, non-specific interactions, e.g., by cytosolic RNA in the
363 pulldowns of ^{H2}F1.
364
365 **Figure 5. *In vivo* analyses of ^{H2}F1 terminal deletion and Znf4 mutants. (A)** IgG pulldowns of
366 N and C truncation mutants (ΔN and ΔC) that removed Znf1-3 and Znf4-8, respectively, and the
367 Znf4 R/K>A substituted (Z4) variant. Association of the constructs with endogenous REH2, ^{H2}F1
368 and REL1 was examined. Cartoon of ^{H2}F1 with zinc fingers and a line marking the N and C
369 truncations. **(B)** qRT-PCR quantitation of RNA transcripts in the pulldowns in panel A. dCq of
370 IgG pulldowns of tagged protein (induced extract) normalized to a mock pulldown (uninduced
371 extract) [dCq = $2^{(\text{test Cq} - \text{mock Cq})}$] for each construct. The mutant proteins were then normalized to
372 the tagged WT protein. All values took into account the recovery of tagged protein in each
373 pulldown. Three independent biological replicates with Cq average values and one standard
374 deviation (+/-1 SD, *n*=3) were plotted. The replicates suggest a similar quality and loading of
375 samples in the pulldowns. Non-specifically associated cytosolic transcripts differed substantially
376 in pulldowns of different mutants, so these transcripts were not used as reference. Mitochondrial
377 unedited (UE) and edited (ED) and cytosolic RNA transcripts are indicated. 1390 and 1400 are
378 abbreviations for the cytosolic HGPRT isoforms Tb927.10.1390 and Tb927.10.1400,
379 respectively.
380

381 ## Analysis of recombinant REH2 *in vitro*
382
383 The conserved predicted catalytic domains in REH2, the impact of mutating catalytic amino
384 acids *in vivo*, and the observed unwinding activity of pulldowns of REH2 and ^{H2}F1 from extracts
385 indicate that REH2 in the context of its native subcomplex in trypanosomes functions as an RNA

386 helicase (3, 4, 22). However, the unwinding activity of the isolated REH2 has not been formally
387 established. We have now generated a recombinant full-length rREH2 polypeptide (240 kDa) that
388 supports robust ATP-dependent unwinding of a synthetic dsRNA substrate *in vitro.* This dsRNA
389 substrate is a mimic of the native A6 editing system formed by pre-annealing of a 3' fragment of
390 the pre-mRNA A6 with a cognate gRNA. The synthetic A6 mRNA/gRNA pair supports a full
391 round of U-deletion editing in an *in vitro* assay with cell extracts and purified RECC enzyme (26,
392 27). The unwinding activity of the recombinant enzyme increased in a titration with increasing
393 concentrations of rREH2, and also in a time course up to 30 min when most of the annealed
394 radiolabeled RNA was unwound (Figs. 6A-B). An upshift of radiolabeled RNA in a ribonucleoprotein
395 complex at the highest tested concentrations of rREH2 in the titration may be due to the known RNA
396 binding activity of the native REH2 established by UV crosslinking (5, 22). The shifted species is
397 sensitive to proteinase K (data now shown). The radiolabeled strand alone (gRNA) and in heat-
398 treated controls of the dsRNA substrate exhibit the same gel mobility as the helicase-unwound gRNA
399 (Figs. 6B-C). Interestingly, a N-terminal truncated rREH2 polypeptide that lacked both dsRBDs was
400 inactive *in vitro* (data not shown). In summary, the isolated 240 kDa recombinant REH2 is a *bona fide*
401 RNA helicase enzyme *in vitro*, and further supports the idea that REH2 may remodel RNA or its
402 RNPs in editing.
403
404 **Figure 6. Recombinant rREH2 is a catalytically active RNA helicase. (A)** Unwinding assays
405 in 10 μL reaction mixtures with increasing concentrations of rREH2[30-2167] +/- ATP; **(B)**
406 Unwinding assays at increasing incubation times with rREH2[30-2167] +/- ATP using the
407 standard reaction mixture described in the material and methods section. The standard reaction
408 used a molar excess of enzyme over substrate. The dsRNA (ds) was assembled by pre-
409 annealing of synthetic transcript that mimics a 3' fragment of the *T. brucei* A6 pre-edited mRNA
410 and a radiolabeled cognate guide RNA (26). Radiolabeled unwound ssRNA (ss) is indicated.
411 Input dsRNA was heat denatured (Δ) as control. **(C)** Additional controls showing that the starting

412 radiolabeled ssRNA used to generate the dsRNA substrate in the assay and the unwound
413 radiolabeled ssRNA in the heat-denatured (Δ) dsRNA (in panel B) have the same gel mobility.
414

415 Discussion

416
417 In the current study, we generated and characterized over 20 constructs of REH2 and ^{H2}F1
418 (Tables 1 and 2) to identify features in these editing proteins that impact the stability of REH2, the
419 assembly of the REH2C RNP, and its RNA-mediated coupling with other components of the RNA
420 editing holoenzyme (or RNA holo-editosome). We also formally established that the isolated REH2 is
421 a *bona fide* RNA helicase enzyme.
422
423 The core RECC enzyme and its accessory *trans* factors RESC and REH2C that assemble
424 around mRNA exhibit transient and stable contacts with each other via RNA. Also, variants of RECC
425 or the GRBC and REMC modules in RESC are emerging in studies by different labs (reviewed in 1).
426 These variants imply a dynamic nature of holo-editosomes that may be important in editing control
427 and needs further characterization. The helicase complex REH2C exhibits transient and stable
428 contacts with variants of RESC that minimally differ in the relative content of MRB3010 (in the GRBC
429 module). In this study, we focused on stable interactions by REH2C that can be readily examined.
430 Prior studies *in vivo* showed that inactivating mutations in the helicase ATP binding site or the
431 dsRBD2 domain dissociate REH2 from GAP1, gRNA and mRNA, reflecting a general helicase
432 detachment from the editing apparatus (3). ^{H2}F1 RNAi dissociates the helicase from the canonical
433 RESC markers GAP1 and RGG2. The RNAi knockdown of either ^{H2}F1 or REH2 inhibits editing
434 associated with a RESC variant that is particularly active and transiently interacts with the helicase
435 REH2 (3, 4). These and other observations indicate that transient and stable contacts in dynamic
436 holo-editosomes including those involving REH2C are important.

437 The section below discusses examined mutations in REH2 and ^{H2}F1 in the current study that
438 identified features affecting the proper assembly of the REH2C RNP, or its association with other
439 components of holo-editosomes *in vivo.*
440

441 **REH2 mutants *in vivo***
442
443 The NTR truncations examined here (>1000 residues each), ∆N and ∆Nds, exhibited a
444 reduced binding with ^{H2}F1 and reduced RNA-mediated association with GAP1. The only difference
445 between these constructs is that ∆N carries the ~70 amino acid dsRBD2 domain but ∆Nds does not.
446 The dsRBD2 is necessary for the proper assembly of REH2 in holo-editosomes (3). Also, the
447 dsRBD2 in the related helicase MLE in flies seems to provide a major RNA-binding surface,
448 presumably due to its potential to bind A-form double helical RNA (28, 29). The tested truncations
449 suggests that other N-terminal features besides dsRBD2, e.g., dsRBD1 or unidentified motifs
450 contribute to normal interactions by REH2 *in vivo*. These truncations may also introduce changes in
451 topology that alter the normal REH2 interactions. Conformational changes are known to modulate
452 functional interactions by other eukayotic DExH/RHA helicases (18, 30). Thus, the tested NTR
453 truncations may indicate the presence of unidentified protein features or global changes in
454 conformation that affect the REH2 interactions. Further studies will be needed to resolve these
455 possibilities. However, relatively short CTR truncations and specific point mutations discussed below
456 also affected the REH2 interactions with other editing components. These short truncations and
457 particularly point mutations in the C-terminus are less likely to cause major conformation changes in
458 REH2.
459
460 We have speculated that the highly conserved OB fold in DExH/RHA subfamily helicases
461 may share functional residues in kinetoplastid RNA editing and other RNA processes (14). Our
462 examined C-terminal truncations included most of the CTR (260 residues in ∆OB) or elements

463 beyond the OB fold that may be specific of REH2 (123 residues in ΔAOB). The conserved and
464 specific C-terminal features of REH2 could work in synergy. We compared specific conserved
465 residues in REH2 and in helicase Prp43p in yeast spliceosomes. R1979 and R2023 in REH2
466 (R664 and R708 in the RNA helicase Prp43p) (16) should be located in two critical loops, β1-β2
467 and β4-β5, respectively. In yeast, R664 and R708 are poised to interact with the RNA substrate
468 entering the helicase cavity, and mutation of either residue inhibits the RNA binding and RNA-
469 mediated activation of Prp43p (16). In trypanosomes, the R2023A substitution had a moderate
470 effect on the stable association of REH2C with GAP1. However, R1979A did not evidently affect
471 this interaction. Neither R1979A or R2023A seem to significant effect on the REH2 interaction
472 with ^{H2}F1.

473 Similarly, H1998 and R1999 in REH2 were compared to the equivalent H1032 and
474 K1033 positions in the RNA helicase MLE in flies. The later residues in MLE bind specific
475 uridylates in U-rich roX boxes of the cognate roX RNA. H1032 and K1033 are also required for
476 the proper function and chromosomal localization of MLE in the *Drosophila* dosage
477 compensation complex (18). The H1998E substitution had a moderate effect on the REH2
478 association with GAP1 but had little or no effect on the interaction with ^{H2}F1. In contrast, the
479 adjacent substitution R1999E affected both the direct REH2 interaction with ^{H2}F1 and the RNA-
480 based REH2 association with GAP1. These results are consistent with a propose role of ^{H2}F1 as
481 an adaptor protein of REH2 (4). So, structure-function correlations may be tractable to specific
482 conserved helicase amino acids in protozoa and vertebrate species. This is in line with the idea
483 that the OB fold in DExH/RHA helicases, including REH2, is a conserved regulatory domain.
484

485 **^{H2}F1 mutants *in vivo***
486
487 ^{H2}F1 has eight predicted C2H2 Znf domains that are spread out and cover over ~45% of the
488 polypeptide sequence. Apart from the Znf domains, ^{H2}F1 has no evident sequence or structural

489 conservation outside of the kinetoplastids. ^{H2}F1 is as an adaptor protein that brings the REH2 to the
490 editing machinery (4) and it is also a stabilizing factor of REH2. That is, the induced downregulation
491 of ^{H2}F1 caused fragmentation of REH2 (4), and we showed here that the converse upregulation of
492 ^{H2}F1 increased the steady-state level of REH2 *in vivo*. ^{H2}F1 may require most of its zinc fingers to
493 stabilize REH2 because substitution of core residues or variable basic residues in individual fingers
494 compromised this function. Thus, ^{H2}F1 binding to REH2 may induce substantial changes in the
495 helicase conformation and stability. The stabilizing role of ^{H2}F1 may involve the coordinated topology
496 of its zinc fingers. Notably, all examined ^{H2}F1 substitution-mutants were able to associate with REH2,
497 GAP1, and REL1. So, the basic fold or positive charge of the fingers is not essential for the
498 association of ^{H2}F1 with other editing components. However, N- or C-terminal truncation of nearly half
499 the size of ^{H2}F1 hampered its normal interactions with the examined editing components. Additional
500 studies are needed to pinpoint specific determinants for ^{H2}F1 direct binding to REH2 or its RNA-
501 mediated contacts with other editing components.

502 Besides the REH2•^{H2}F1 system, other DExH/RHA helicase•Znf protein pairs have been
503 characterized (14): the MOP•MEP-1 system in worm embryogenesis, and the DXH30•ZAP system in
504 antivirus protection in humans (31, 32). The antiviral protein ZAP has four Znf motifs that participate
505 in viral RNA recognition (32). All four fingers are on a positively charged surface in a crystal structure
506 of ZAP (24). and substitution of the basic residues in the fingers inhibited the antiviral functions of
507 ZAP (32). Insights from the ZAP structure imply that stabilization of REH2 by ^{H2}F1 involves a precise
508 topology of its zinc fingers and a role of its fingers in RNA binding. Notably, the Znf proteins ZAP and
509 MEP-1 multimerize. If ^{H2}F1 dimerizes as it was shown for recombinant ZAP (24) a single REH2C
510 RNP would include 16 zinc fingers. The co-purification of tagged and endogenous ^{H2}F1 from RNase-
511 treated extracts suggest the presence of direct protein contacts between the ^{H2}F1 copies (S3 Fig.).
512 However, analyses of recombinant ^{H2}F1 are necessary to establish the potential of ^{H2}F1 to
513 multimerize or bind RNA. The RNA content in pulldowns of a ^{H2}F1 variant with four R/K>Ala
514 substitutions in Znf4 suggested minimal changes in association with target RNAs in mitochondria but

515 a significance loss in non-specific contacts with unrelated transcripts. So, subtle changes in RNA
516 affinity are more likely to affect weak non-specific RNA contacts. The dramatic loss of all transcripts
517 examined in the pulldowns of the tested ^{H2}F1 fragments suggest that efficient RNA association by the
518 REH2C subcomplex *in vivo* requires the full array of zinc fingers in ^{H2}F1. Unfortunately, we were
519 unable to maintain stable expression an ^{H2}F1 construct with mutations in all fingers or subsets of
520 fingers (data not shown). We note that the transcripts examined may associate with either ^{H2}F1,
521 REH2 or both proteins in the native REH2C RNP.
522

523 **REH2 may function as an RNA helicase in kinetoplastid RNA editing**
524
525 Prior studies support the idea that REH2 is a functional RNA helicase in the context of the
526 editing apparatus. That is, REH2 pulldowns from GAP1-depleted extracts exhibit RNA unwinding
527 activity. Also, mutation of conserved catalytic residues in the predicted RecA1 domain inhibits the
528 unwinding activity of REH2 pulldowns from mitochondrial extracts (22). We have now established
529 that the isolated full-length recombinant REH2 (240 kda) is a *bona fide* RNA helicase enzyme.
530 Additional studies are needed to determine if ^{H2}F1 affects the unwinding activity of REH2. Thus,
531 REH2, the only DExH/RHA-type RNA helicase in kinetoplastid holo-editosomes most likely provides
532 an ATP-dependent unwinding activity in RNA editing. Besides REH2, the editing apparatus also
533 requires the DEAD-box RNA helicase REH1 (12, 13). This helicase is not considered to be a subunit
534 of the RNPs studied here and no potential binding partner of REH1 has been identified. A transient
535 RNA-mediate interaction of REH1 with other editing proteins has been detected (22, 33).
536 Important functional differences are known between the two ATP-dependent RNA helicases.
537 REH2 is needed for editing within single blocks, including the first “initiating” block (3). In
538 contrast, REH1 is needed for editing of two or more blocks (i.e., by overlapping gRNAs) but has
539 no effect on the first block (13). Both RNA helicases may be involved in critical remodeling of
540 RNA or RNP structure. REH1 may promote the relay of gRNAs as editing progresses from one

541 block to the next. Our ongoing RNA-seq analyses suggest that REH2 may impact the editing
542 efficiency at the individual sites and may provide additional functional insights concerning
543 REH2C (Kumar et al., unpublished).
544

545 Possible roles of editing complex variants
546
547 The editing apparatus much like the splicing and transcription molecular machines may
548 exhibit dynamic phases of assembly and function. The native RECC enzyme has multiple
549 isoforms, and several RNase III-like protein subunits in RECC predict a binary combinatorial
550 potential that may add fine-tuning in editing function (34-36). Also, natural GRBC and REMC
551 isoforms and genetically-induced changes in the organization of their protein and RNA
552 components are emerging. A recurring theme in the known examples is the variable interaction
553 between the GAP1/2 heterotetramer that is required for all editing involving GRBC-bound
554 gRNAs, and MRB3010 (GRBC6) that participates in early editing (1, 6, 37). A controlled
555 interaction of the GAP1/2 tetramer with MRB3010 may be used to modulate editing. For
556 example, GRBC variants in direct pulldowns of MRB3010 or REH2 pulldowns differ in their
557 relative content of MRB3010 and editing level in examined associated mRNAs (3, 5). However,
558 RNAi of REH2 or ^{H2}F1 reduced the editing level in mRNAs in the MRB3010 pulldowns (3, 4).
559 REH2 and ^{H2}F1 features, including those examined in the current studies, are expected to affect
560 specific steps in the editing mechanism and current studies in our lab are addressing this.
561 Variations in MRB3010 or other critical RESC proteins may distinguish pre-editosomes from
562 fully-active editosomes. Dynamics in complex assembly could also pause editing facilitating
563 helicase remodeling of RNA or RNPs. Additional studies are needed to examine these
564 possibilities in editing control.
565

566 # Materials and methods
567
568 ## Cell Culture
569
570 *T. brucei* Lister strain 427 29-13 procyclic was grown axenically in log phase in SDM79
571 medium (38) and harvested at a cell density of 1–3x10^7 cells/mL. All transgenic cell lines were
572 induced with tetracycline at 1µg/mL. The TbRGG2 (alias RGG2) RNAi cell line was provided by
573 the Read lab (39). The GAP1 and ^{H2}F1 RNAi cell lines that were used as controls in some
574 analyses were generated in our lab (3, 4). We have seen that the TAP tag in REH2 or ^{H2}F1,
575 including WT constructs, seems to slow the growth of trypanosomes after several days of
576 culture (22)(data not shown). This and presumably incomplete cloning after transfection may
577 account for the uneven expression levels in extracts from independent subcultures. To partially
578 control for this issue, most plasmid constructs in the current study were re-made to use
579 puromycin selection. Transfections were also repeated with tetracycline-screened HyClone
580 Fetal Bovine Serum (FBS) (SH30070.03T; GE Healthcare. This enabled a faster cell recovery
581 after transfection than with constructs using phleomycin selection that were originally
582 characterized (data not shown). Regardless of this issue, independent analyses of protein
583 (complex) interactions were consistent with either puromycin or phleomycin constructs.
584

585 ## DNA constructs
586
587 All overexpression and RNAi studies used inducible plasmid constructs. The constructs
588 for ^{H2}F1 RNAi and the REH2 dsRBD2 mutant K1078A/A1086D were previously reported (3, 4).
589 N-terminal deletion constructs for REH2 (ΔN and ΔNds) and ^{H2}F1 (ΔN) were prepared using the
590 In-Fusion® HD Cloning Kit (639648; Clontech). Two PCR amplicons were prepared in each
591 case using CloneAmp™ HiFi PCR Premix (638500; Clontech) and were then gel-eluted using
592 NucleoSpin® Gel and PCR Clean-up (740609.10; Clontech). One amplicon encodes the first 34
593 amino acids of REH2 (primers: F-1503, R-1522), including the predicted REH2 mitochondrial

594 leader sequence (REH2-MLS) (22), that was used for all N-deletion constructs. The other
595 amplicon included the remaining relevant gene fragment sequence: 3070-6501 bases (REH2
596 ΔN), 3280-6501 bases (REH2 ΔNds), or 766-1572 bases (^{H2}F1 ΔN). Three-piece in-fusion
597 reactions were performed to join the two amplicons and pLEW79-ada-TAP plasmid linearized at
598 *XhoI* and *BamHI* (40). The PCR primers (S1 Table) included 5' and 3' terminal homology (15
599 bases) to enable the recombination-based fusion between the amplicons and the plasmid DNA.
600 The REH2 (ΔAOB and ΔOB) and ^{H2}F1 ΔC deletion constructs are also recombination-based
601 fusions of the amplified relevant gene fragment with linearized plasmid DNA. The REH2
602 constructs R2023A, H1998E, R1999E and H1998E/R1999E, and the ^{H2}F1 constructs Z5 C>A
603 and Z5 R/K>A, were created by site-directed mutagenesis in inverse-PCR reactions of the
604 pLEW79-ada-TAP WT plasmid as the template. pLEW79-ada-TAP was modified from the
605 original pLEW79-TAP (40, 41). The resulting linearized mutant constructs were circularized
606 using the In-Fusion HD Cloning Kit. Other ^{H2}F1 constructs used synthetic gBlock gene
607 fragments (IDT) with mutations in single or multiple zinc-fingers. The gBlock fragment
608 sequences were fused as follows. A full-length ^{H2}F1 sequence with all fingers mutated (Z1-8
609 C>A) was cloned into *XhoI/BamHI* sites of the plasmid vector. N-terminal fragments of ^{H2}F1 (Z1,
610 Z2 and Z3 R/K>A single finger mutants) replaced the corresponding sequence in the ^{H2}F1 WT
611 construct after digestion with *XhoI* and the internal *ApaI* site in ^{H2}F1. C-terminal fragments of
612 ^{H2}F1 (Z4 and the multi-finger mutant Z6-Z8) replaced corresponding sequence in the ^{H2}F1 WT
613 construct after digestion with *ApaI* and *BamH1*. All constructs were confirmed by DNA
614 sequencing, linearized with *NotI*, and transfected in trypanosomes (38).
615

616 **Western Blots and Radioactivity Assays**
617
618 Western blots of REH2, ^{H2}F1 and ^{H2}F2 (subunits of REH2C), GAP1 (alias GRBC2;
619 subunit of GRBC) and A2 (alias MP42; subunit of RECC) were performed as reported (4, 22).

620 Western blots of the GAP1/GAP2 (alias GRBC2/GRBC1) paralogs simultaneously, and of
621 MRB8170 and MRB6070 (subunits of REMC and MRB6070/1590 assemblies, respectively),
622 were performed as previously described (42, 43). Peroxidase Anti-peroxidase antibody (P1291;
623 Sigma) diluted to 1:200 (v/v) was used to detect the TAP-tag. Protein quantitative analyses
624 using Amersham ECL^{TM} western blot detection reagents were performed in an Amersham
625 Imager 600. RNA ligases in the RECC enzyme were radiolabeled by self-adenylation directly on
626 the beads in IgG pulldowns (44). Unwinding assays of REH2 used reported conditions with a
627 few modifications (4) and full-length recombinant His-REH2. The dsRNA substrate in these
628 assays used an A6 mRNA/gRNA pair (22). The A6 pair mimics the endogenous ATPase subunit
629 6 substrate. The gRNA was transcribed with RNA T7 polymerase from an amplicon (S1 Table)
630 after *DraI* restriction digestion and gel purification of the product. The 61-nt gRNA was 5'-
631 labelled with γ^{32}P-ATP using T4 Polynucleotide kinase. The 62-nt mRNA was synthetic (IDT). A
632 mix with 3 pmoles of labelled gRNA and 15 pmoles of mRNA was heated at 95° C for 3 min,
633 and then immediately incubated for 30 min at room temperature in the annealing buffer (10 mM
634 MOPS pH 6.5, 1 mM EDTA, and 50 mM KCl). The annealed RNA hybrids were isolated from
635 native 12% PAGE run at 4 ˚C at 50 V for 120 min in 0.5x Tris-borate-EDTA buffer. Standard 10
636 μL reaction mixtures in unwinding buffer (40 mM Tris-Cl pH 8.0, 0.5 mM $MgCl^2$, 0.01% Nonidet
637 P-40, and 2 mM DTT) were incubated for 30 min at 19 °C with 20 cps of hybrid (~20 fmoles)
638 and 3 µg of recombinant REH2 (~12 pmoles). Variations to the standard assay including in the
639 concentration of REH2 or the reaction time are indicated in the text. All assays contained 100
640 fmoles of unlabeled gRNA as competitor to prevent re-annealing of unwound γ^{32}P-gRNA. The
641 assays were stopped with an equal volume of 2x helicase reaction stop buffer (50 mM EDTA,
642 1% SDS, 0.1% bromophenol blue, 0.1% xylene cyanol, and 20% glycerol) and kept on ice for 5
643 min. The assays in Fig. 6B were also treated with 0.4U of proteinase K (P8107S; NEB), 25 mM

644 EDTA and 0.5% SDS at 22° C for 30 min. The entire reaction was loaded onto a native 12%
645 PAGE and resolved at 25 V for 120 min at 4°C.
646

647 **Cell extracts and purification of protein and RNA from IgG pulldowns**
648
649 Whole cell extracts as well as mitochondria-enriched extracts were used in this study.
650 Whole-cell extracts were generated by incubation of cell pellets in MRB-Triton buffer (25 mM
651 Tris-Cl pH 8.0, 10 mM MgOAC, 1 mM EDTA, 10 mM KCl, 5% glycerol, 0.5% Triton X-100) at 4
652 °C for 45 minutes followed by centrifugation at 15,000g for 30 minutes. Mitochondria-enriched
653 extracts were prepared using a simplified protocol similar to others reported earlier (2, 45).
654 Namely, cell pellets were resuspended into hypotonic DTE buffer (1 mM Tris-HCl pH 8.0, 1 mM
655 EDTA pH 8.0) supplemented with protease inhibitors and disrupted in a Dounce homogenizer.
656 The suspension was passed through a 26-gauge needle as originally described (46). The
657 enriched mitochondrial vesicles were spun down and the cytosolic content in the supernatant
658 discarded. This step improved the recovery of intact REH2 compared to whole-cell extracts.
659 REH2 is more prone to fragmentation than other proteins examined in this study. The following
660 steps were also as in (46). The pellet was resuspended into STM buffer (0.25M Sucrose, 20 mM
661 Tris-HCl pH 8.0, 2 mM $MgCl_2$) supplemented with DNase I, RNase-free (EN0523; Fisher
662 Scientific). The reaction was stopped with one volume of STE buffer (0.25 M Sucrose, 20 mM
663 Tris-HCl pH 8.0, 2 mM EDTA pH 8.0). The enriched mitochondria were spun down and washed
664 in STE buffer. The pellet was resuspended into MRB-Triton buffer and incubated in ice for 15
665 min. The suspension was spun down at 15,000g at 4 °C for 30 min. The supernatant was
666 collected and stored at -80 °C. In IgG pulldowns of the extracts, ectopically expressed TAP-
667 REH2 and TAP-^{H2}F1 were recovered as reported (4, 22) with some modifications.
668 Approximately 2 mg of protein was mixed with 1x SUPERase·In™ RNase inhibitor (Invitrogen™)
669 and incubated with Dynabeads IgG (11203D; Invitrogen™). The beads were washed five times

670 with 1ml of wash buffer (150 mM NaCl, 1 mM EDTA, 10 mM MgAOc, 0.1% NP-40, and 25 mM
671 Tris pH 8.0). Protein was eluted from the beads with 15 μL of 1x SDS loading buffer at 95 °C for
672 2 min. RNA was extracted by treating the beads with 4U proteinase K (NEB) for 2 hrs at 55 °C,
673 followed by phenol extraction and ethanol precipitation. For some pulldowns, RNase A/T1 mix
674 (EN0551; Fisher Scientific) was applied at 20 U/mg of protein both in the input extract and again
675 while bound to the beads.
676

677 **Quantitative RT-PCR**
678
679 Isolated RNA from the pulldowns or directly from input extracts was treated with DNase
680 I, RNase-free (EN0523; Thermo Scientific™) prior to cDNA synthesis with the iScript™ Reverse
681 Transcription Supermix (Bio-Rad) as described elsewhere (5). The amplifications mixtures (10
682 µl) used SsoAdvanced™ Universal SYBR® Green Supermix (Bio-Rad) and reported
683 oligonucleotides for unedited mRNAs, fully edited mRNA, and reference transcripts (47). Diluted
684 samples of the examined cDNA produced a single amplicon during linear amplification under
685 our conditions. The end-point amplicons described here have been gel-isolated, cloned and
686 confirmed by sequencing (5) (data not shown). Fold-enrichment of mitochondrial and cytosolic
687 transcripts in IgG pulldowns of tagged proteins (induced extracts), relative to a mock pulldown
688 (uninduced extract), was calculated as follows: Fold = $2^{[-ddCq]}$, where ddCq = Cq test IP – Cq
689 mock IP, as in (5). The relative value for each mutant construct was adjusted to the amount of
690 recovered tagged protein, and subsequently normalized to the tagged WT construct (= 1). The
691 plot in Fig. 5B was constructed using data from 3 independent biological replicate experiments,
692 including a total of six amplicons per data point (i.e., two technical replicate amplicons per
693 assay). Two of the independent experiments (including cultures +/- Tet for each mutant) were
694 performed concurrently. The third independent experiment (one set of cultures per mutant +/-
695 Tet) was conducted on a subsequent date. The replicate experiments showed a consistent

696 sample loading in the assays used in our plots. The examined mutant constructs differed in the
697 amount of non-specific association with Tubulin and other cytosolic transcripts that are normally
698 used as internal reference in antibody pulldowns using a common protein bait. The raw Cq
699 values of examined editing transcripts in the pulldowns and the plotted values after
700 normalization indicated a substantial loss of these transcripts in the truncated mutants.
701 qRT-PCR assays of input extract in S4 Fig. were normalized using the following equation: Ratio
702 (reference/target) = $2^{[Cq(ref) - Cq(target)]}$. This scores the relative difference between the reference
703 and target Cq values. The current plots of input extract used 18S rRNA as reference (S4 Fig.).
704 Similar results were obtained with any of these cytosolic transcripts used as a reference: tubulin,
705 1400 or 1390 (Tb927.10.1400 or Tb927.10.1390, respectively) (data not shown).
706

707 **Homology modeling and bioinformatic analysis**
708
709 The multiple-sequence alignment of REH2 and MLE was done with Clustal Omega (48),
710 and that of the ^{H2}F1 zinc finger domains was done with BOXSHADE version 3.21
711 (http:/www.ch.embnet.org/software/BOX_form.html). The homology models of the helicase
712 region of *T. brucei* REH2 were built using the program Phyre2 (20).
713

714 **Recombinant protein**
715
716 6xHis-REH2 (amino acid residues 30-2167) was amplified by PCR (S1 Table). The gel-
717 purified product was cloned into the NcoI and BamHI sites in the expression vector pET15b by
718 using the NEBuilder® HiFi DNA Assembly Master Mix (E262, NEB) and the appropriate primers.
719 The ligation reaction mixtures were transformed into chemically competent Omnimax cells from
720 ThermoFisher Scientific. Colonies with the correct insert were identified by single-colony PCR
721 and then amplified for plasmid purification. The sequence of the flanking vector region and the
722 insert was checked by DNA sequencing. The plasmid DNA was transformed into Rosetta2 DE3
723 cells (Novagen Inc.) and overexpressed in 4 L of Terrific Broth media by supplementing 2% (v/v)

724 ethanol and 2 mM $MgCl_2$ at 37 °C. Protein induction with 0.5 mM IPTG was done at a OD_{600} of
725 0.8, and the expression was continued for 22 hours at 16 °C. The cell pellet was stored at -80
726 °C overnight and was resuspended in lysis buffer (5 mL/g of cell pellet) of 50 mM Tris-HCl pH
727 8.0, 250 mM NaCl, 1 mM EDTA, and 1 mM DTT along with 10 µg of RNase-free DNase and 15
728 mg of hen egg white lysozyme. The cells were lysed in an Emulsiflex hydraulic press. The cell
729 debris was pelleted at 39,200 x g for 30 minutes at 4 °C. The supernatant with 6xHis-REH2 was
730 batch attached to equilibrated Qiagen Ni-NTA Agarose at 4 °C for 16 hrs. The complex was
731 eluted with 50 mM Tris-HCl pH 8.0, 300 mM NaCl, 1 mM DDT, and 250 mM imidazole. The first
732 elution of the purification was dialyzed into unwinding assay buffer. This material was tested for
733 the presence of the recombinant protein in western blots and antibody pulldowns, and for
734 activity in dsRNA unwinding activity assays *in vitro*.
735

736 # Acknowledgements
737

738 We thank the Read lab for their gift of antibodies against GAP1, TbRGG2 (alias RGG2)
739 and ^{H2}F2. The Afasizhev lab kindly provided antibodies that react against the GAP1/GAP2
740 paralogs (alias GRBC2/GRBC1) simultaneously. We also thank the Stuart lab for providing the
741 antibodies against A2 (alias MP42). Amna Mushtaq provided detailed comments on the
742 manuscript. Jana Gomez, Elizabeth Alvarez and Melissa Yang helped with the preparation of
743 figures.
744
745
746
747

748 # References
749

750 1. Cruz-Reyes J, Mooers BHM, Doharey PK, Meehan J, Gulati S. Dynamic RNA
751 holoeditosomes with subcomplex variants: Insights into the control of trypanosome editing.
752 WIREs RNA. 2018;e1502.
753 2. Koslowsky DJ, Sun Y, Hindenach J, Theisen T, Lucas J. The insect-phase gRNA
754 transcriptome in Trypanosoma brucei. Nucleic acids research. 2013.
755 3. Madina BR, Kumar V, Mooers BH, Cruz-Reyes J. Native Variants of the MRB1 Complex
756 Exhibit Specialized Functions in Kinetoplastid RNA Editing. PloS one. 2015;10(4):e0123441.
757 4. Kumar V, Madina BR, Gulati S, Vashisht AA, Kanyumbu C, Pieters B, et al. REH2C
758 Helicase and GRBC Subcomplexes May Base Pair through mRNA and Small Guide RNA in
759 Kinetoplastid Editosomes. J Biol Chem. 2016;291(11):5753-64.
760 5. Madina BR, Kumar V, Metz R, Mooers BH, Bundschuh R, Cruz-Reyes J. Native
761 mitochondrial RNA-binding complexes in kinetoplastid RNA editing differ in guide RNA
762 composition. RNA. 2014;20(7):1142-52.
763 6. Aphasizheva I, Zhang L, Wang X, Kaake RM, Huang L, Monti S, et al. RNA binding and
764 core complexes constitute the U-insertion/deletion editosome. Mol Cell Biol. 2014;34(23):4329-
765 42.
766 7. Huang Z, Faktorova D, Krizova A, Kafkova L, Read LK, Lukes J, et al. Integrity of the
767 core mitochondrial RNA-binding complex 1 is vital for trypanosome RNA editing. RNA. 2015.
768 8. McAdams NM, Simpson RM, Chen R, Sun Y, Read LK. MRB7260 is essential for
769 productive protein-RNA interactions within the RNA editing substrate binding complex during
770 trypanosome RNA editing. RNA. 2018;24(4):540-56.
771 9. Simpson RM, Bruno AE, Bard JE, Buck MJ, Read LK. High-throughput sequencing of
772 partially edited trypanosome mRNAs reveals barriers to editing progression and evidence for
773 alternative editing. RNA. 2016;22(5):677-95.

774 10. Simpson RM, Bruno AE, Chen R, Lott K, Tylec BL, Bard JE, et al. Trypanosome RNA
775 Editing Mediator Complex proteins have distinct functions in gRNA utilization. Nucleic acids
776 research. 2017;45(13):7965-83.
777 11. Shaw PL, McAdams NM, Hast MA, Ammerman ML, Read LK, Schumacher MA.
778 Structures of the T. brucei kRNA editing factor MRB1590 reveal unique RNA-binding pore motif
779 contained within an ABC-ATPase fold. Nucleic acids research. 2015;43(14):7096-109.
780 12. Missel A, Souza AE, Norskau G, Goringer HU. Disruption of a gene encoding a novel
781 mitochondrial DEAD-box protein in Trypanosoma brucei affects edited mRNAs. Mol Cell Biol.
782 1997;17(9):4895-903.
783 13. Li F, Herrera J, Zhou S, Maslov DA, Simpson L. Trypanosome REH1 is an RNA helicase
784 involved with the 3'-5' polarity of multiple gRNA-guided uridine insertion/deletion RNA editing.
785 Proc Natl Acad Sci U S A. 2011;108(9):3542-7.
786 14. Cruz-Reyes J, Mooers BH, Abu-Adas Z, Kumar V, Gulati S. DEAH-RHA helicase•Znf
787 cofactor systems in kinetoplastid RNA editing and evolutionarily distant RNA processes. RNA
788 Dis. 2016;3(2):e1336.
789 15. Jarmoskaite I, Russell R. RNA helicase proteins as chaperones and remodelers. Annu
790 Rev Biochem. 2014;83:697-725.
791 16. Walbott H, Mouffok S, Capeyrou R, Lebaron S, Humbert O, van Tilbeurgh H, et al.
792 Prp43p contains a processive helicase structural architecture with a specific regulatory domain.
793 EMBO J. 2010;29(13):2194-204.
794 17. Robert-Paganin J, Rety S, Leulliot N. Regulation of DEAH/RHA helicases by G-patch
795 proteins. Biomed Res Int. 2015;2015:931857.
796 18. Prabu JR, Muller M, Thomae AW, Schussler S, Bonneau F, Becker PB, et al. Structure
797 of the RNA Helicase MLE Reveals the Molecular Mechanisms for Uridine Specificity and RNA-
798 ATP Coupling. Mol Cell. 2015;60(3):487-99.

799 19. Dhote V, Sweeney TR, Kim N, Hellen CU, Pestova TV. Roles of individual domains in
800 the function of DHX29, an essential factor required for translation of structured mammalian
801 mRNAs. Proc Natl Acad Sci U S A. 2012;109(46):E3150-9.
802 20. Kelley LA, Mezulis S, Yates CM, Wass MN, Sternberg MJ. The Phyre2 web portal for
803 protein modeling, prediction and analysis. Nat Protoc. 2015;10(6):845-58.
804 21. Jankowsky E. RNA helicases at work: binding and rearranging. Trends in biochemical
805 sciences. 2011;36(1):19-29.
806 22. Hernandez A, Madina BR, Ro K, Wohlschlegel JA, Willard B, Kinter MT, et al. REH2
807 RNA helicase in kinetoplastid mitochondria: ribonucleoprotein complexes and essential motifs
808 for unwinding and guide RNA (gRNA) binding. J Biol Chem. 2010;285(2):1220-8.
809 23. Segal DJ, Crotty JW, Bhakta MS, Barbas CF, 3rd, Horton NC. Structure of Aart, a
810 designed six-finger zinc finger peptide, bound to DNA. J Mol Biol. 2006;363(2):405-21.
811 24. Chen S, Xu Y, Zhang K, Wang X, Sun J, Gao G, et al. Structure of N-terminal domain of
812 ZAP indicates how a zinc-finger protein recognizes complex RNA. Nat Struct Mol Biol.
813 2012;19(4):430-5.
814 25. Klug A. The discovery of zinc fingers and their development for practical applications in
815 gene regulation and genome manipulation. Q Rev Biophys. 2010;43(1):1-21.
816 26. Seiwert SD, Heidmann S, Stuart K. Direct visualization of uridylate deletion in vitro
817 suggests a mechanism for kinetoplastid RNA editing. Cell. 1996;84(6):831-41.
818 27. Rusche LN, Cruz-Reyes J, Piller KJ, Sollner-Webb B. Purification of a functional
819 enzymatic editing complex from Trypanosoma brucei mitochondria. EMBO J. 1997;16(13):4069-
820 81.
821 28. Izzo A, Regnard C, Morales V, Kremmer E, Becker PB. Structure-function analysis of the
822 RNA helicase maleless. Nucleic acids research. 2008;36(3):950-62.
823 29. Masliah G, Barraud P, Allain FH. RNA recognition by double-stranded RNA binding
824 domains: a matter of shape and sequence. Cell Mol Life Sci. 2013;70(11):1875-95.

825 30. Christian H, Hofele RV, Urlaub H, Ficner R. Insights into the activation of the helicase
826 Prp43 by biochemical studies and structural mass spectrometry. Nucleic acids research.
827 2014;42(2):1162-79.
828 31. Ye P, Liu S, Zhu Y, Chen G, Gao G. DEXH-Box protein DHX30 is required for optimal
829 function of the zinc-finger antiviral protein. Protein & cell. 2010;1(10):956-64.
830 32. Guo X, Carroll JW, Macdonald MR, Goff SP, Gao G. The zinc finger antiviral protein
831 directly binds to specific viral mRNAs through the CCCH zinc finger motifs. J Virol.
832 2004;78(23):12781-7.
833 33. Kruse E, Voigt C, Leeder WM, Goringer HU. RNA helicases involved in U-
834 insertion/deletion-type RNA editing. Biochimica et biophysica acta. 2013;1829(8):835-41.
835 34. Carnes J, Soares CZ, Wickham C, Stuart K. Endonuclease associations with three
836 distinct editosomes in Trypanosoma brucei. J Biol Chem. 2011;286(22):19320-30.
837 35. McDermott SM, Luo J, Carnes J, Ranish JA, Stuart K. The Architecture of Trypanosoma
838 brucei editosomes. Proc Natl Acad Sci U S A. 2016;113(42):E6476-E85.
839 36. Carnes J, McDermott S, Anupama A, Oliver BG, Sather DN, Stuart K. In vivo cleavage
840 specificity of Trypanosoma brucei editosome endonucleases. Nucleic acids research.
841 2017;45(8):4667-86.
842 37. Ammerman ML, Hashimi H, Novotna L, Cicova Z, McEvoy SM, Lukes J, et al. MRB3010
843 is a core component of the MRB1 complex that facilitates an early step of the kinetoplastid RNA
844 editing process. RNA. 2011;17(5):865-77.
845 38. Wirtz E, Leal S, Ochatt C, Cross GA. A tightly regulated inducible expression system for
846 conditional gene knock-outs and dominant-negative genetics in Trypanosoma brucei. Molecular
847 and biochemical parasitology. 1999;99(1):89-101.
848 39. Fisk JC, Ammerman ML, Presnyak V, Read LK. TbRGG2, an essential RNA editing
849 accessory factor in two Trypanosoma brucei life cycle stages. J Biol Chem.
850 2008;283(34):23016-25.

851 40. Hernandez A, Panigrahi A, Cifuentes-Rojas C, Sacharidou A, Stuart K, Cruz-Reyes J.
852 Determinants for association and guide RNA-directed endonuclease cleavage by purified RNA
853 editing complexes from Trypanosoma brucei. J Mol Biol. 2008;381(1):35-48.
854 41. Panigrahi AK, Schnaufer A, Ernst NL, Wang B, Carmean N, Salavati R, et al.
855 Identification of novel components of Trypanosoma brucei editosomes. RNA. 2003;9(4):484-92.
856 42. Ammerman ML, Downey KM, Hashimi H, Fisk JC, Tomasello DL, Faktorova D, et al.
857 Architecture of the trypanosome RNA editing accessory complex, MRB1. Nucleic acids
858 research. 2012;40(12):5637-50.
859 43. Weng J, Aphasizheva I, Etheridge RD, Huang L, Wang X, Falick AM, et al. Guide RNA-
860 binding complex from mitochondria of trypanosomatids. Mol Cell. 2008;32(2):198-209.
861 44. Sabatini R, Hajduk SL. RNA ligase and its involvement in guide RNA/mRNA chimera
862 formation. Evidence for a cleavage-ligation mechanism of Trypanosoma brucei mRNA editing. J
863 Biol Chem. 1995;270(13):7233-40.
864 45. Hashimi H, Zikova A, Panigrahi AK, Stuart KD, Lukes J. TbRGG1, an essential protein
865 involved in kinetoplastid RNA metabolism that is associated with a novel multiprotein complex.
866 RNA. 2008;14(5):970-80.
867 46. Harris ME, Hajduk SL. Kinetoplastid RNA editing: in vitro formation of cytochrome b
868 gRNA-mRNA chimeras from synthetic substrate RNAs. Cell. 1992;68(6):1091-9.
869 47. Carnes J, Stuart KD. Uridine insertion/deletion editing activities. Methods in enzymology.
870 2007;424:25-54.
871 48. Sievers F, Higgins DG. Clustal Omega, accurate alignment of very large numbers of
872 sequences. Methods Mol Biol. 2014;1079:105-16.
873
874

875 # Supporting information
876
877 **S1 Fig. Multi-sequence alignment of a C-terminal segment in *T. brucei* REH2 and**
878 ***Drosophila* MLE DExH/RHA RNA helicases**. The alignment was generated with Clustal
879 Omega (48). Boxes were inserted manually to improve the match between the MLE and REH2
880 residues. Note that H1032, K1033 and T1034 (in red), which make U-specific contacts in MLE,
881 are aligned with H1998, R1999 and T2000 (in red) in REH2.
882
883 **S2 Fig. Sedimentation analysis of endogenous editing proteins. (A)** 10-30% glycerol
884 gradients of freshly-made mitochondria-enriched extract from 29:13 procyclic trypanosomes.
885 Catalase and RECC complex were used as 11 S and 20 S markers, respectively (22).
886 Endogenous REH2, ^{H2}F1 and ^{H2}F2, GAP1 (GRBC2), GAP2 (GRBC1), and A2 (MP42) were
887 examined in western blots. All panels in this figure derived from the same extract fractions. The
888 data shown is representative of at least two panels for each protein in biological replicate
889 gradients.
890
891 **S3 Fig. RNase-resistant co-purification of tagged-^{H2}F1 and endogenous ^{H2}F1.** Western
892 blots of IgG pulldowns from extracts with or without an RNaseA/T1 mix. All panels in this figure
893 derive from the same blot. The upper blot with the tagged-^{H2}F1 bait was cut below the 75 kDa
894 marker. The middle and lower panels were divided between the 50 kDa and 37 kDa marker.
895 The 34.4 kDa RGG2, a typical subunit of the REMC module in the RESC complex. As expected,
896 the RNA-mediated association of RGG2 decreased with the RNase treatment.
897
898 **S4 Fig. Quantitation of steady-state RNA transcripts in the input mitochondrial extracts**
899 **used in the IgG pulldowns.** Independent biological replicates (two independent cultures used
900 in **Fig. 5**) with Cq average values and one standard deviation (+/-1SD, *n*=2) were plotted. dCq

901 of steady-state RNA transcripts in lysates relative to background 18s rRNA used as reference
902 [$dCq = 2^{(target\ Cq - ref\ Cq)}$]. Shorter bars indicate a smaller differential versus 18s rRNA in the
903 sample. For example, ND7 is relatively abundant compared to other transcripts in the sample
904 (i.e., it has a lower Cq). The WT construct is induced or not (+/-). All mutants are induced. All
905 end-point amplicons were examined in gels to confirm that they were single products during
906 linear amplification.

907

908 **S1 Table. DNA oligonucleotides, gBlocks (IDT) and synthetic RNA.**

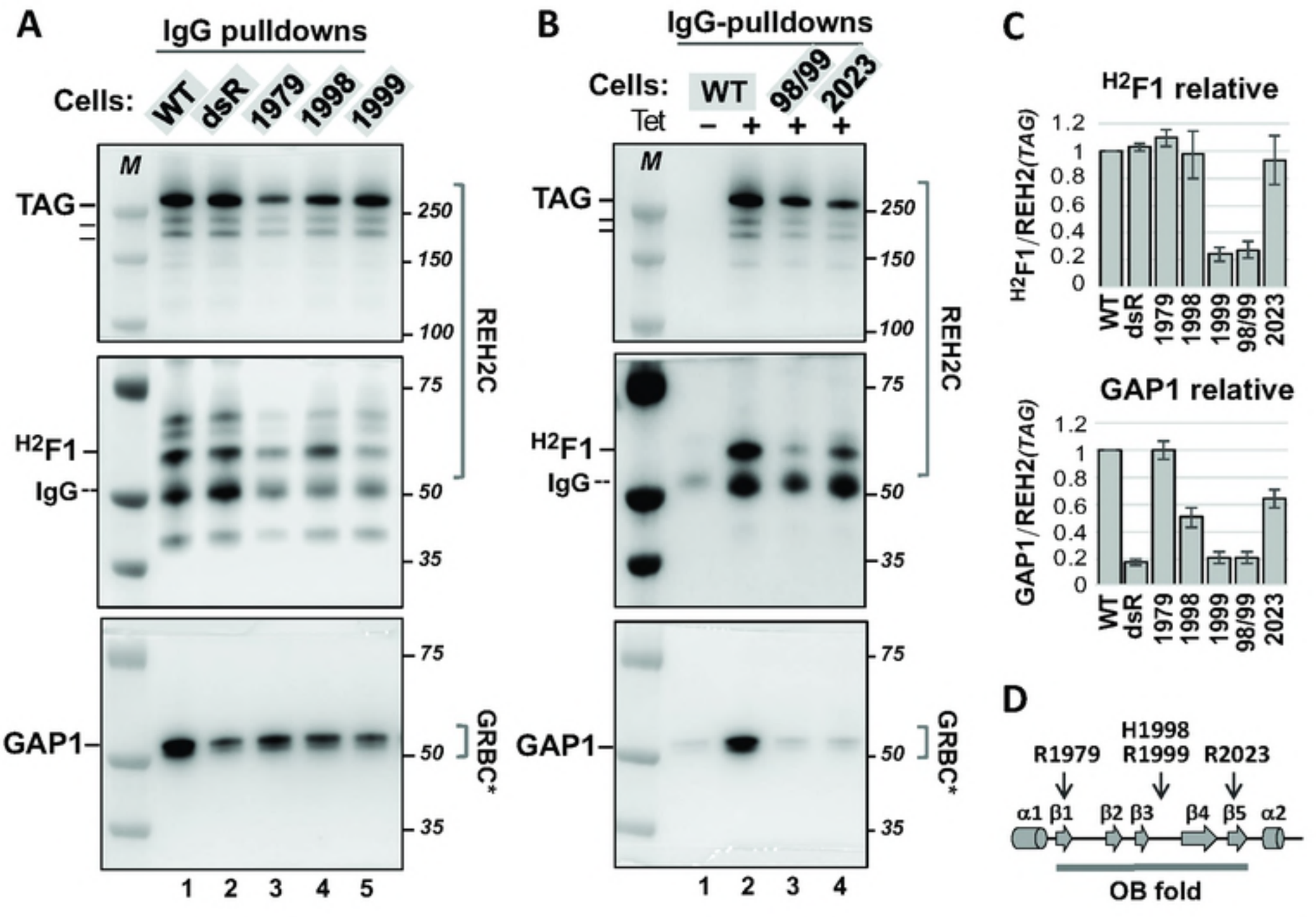

Figure 2

Figure 2

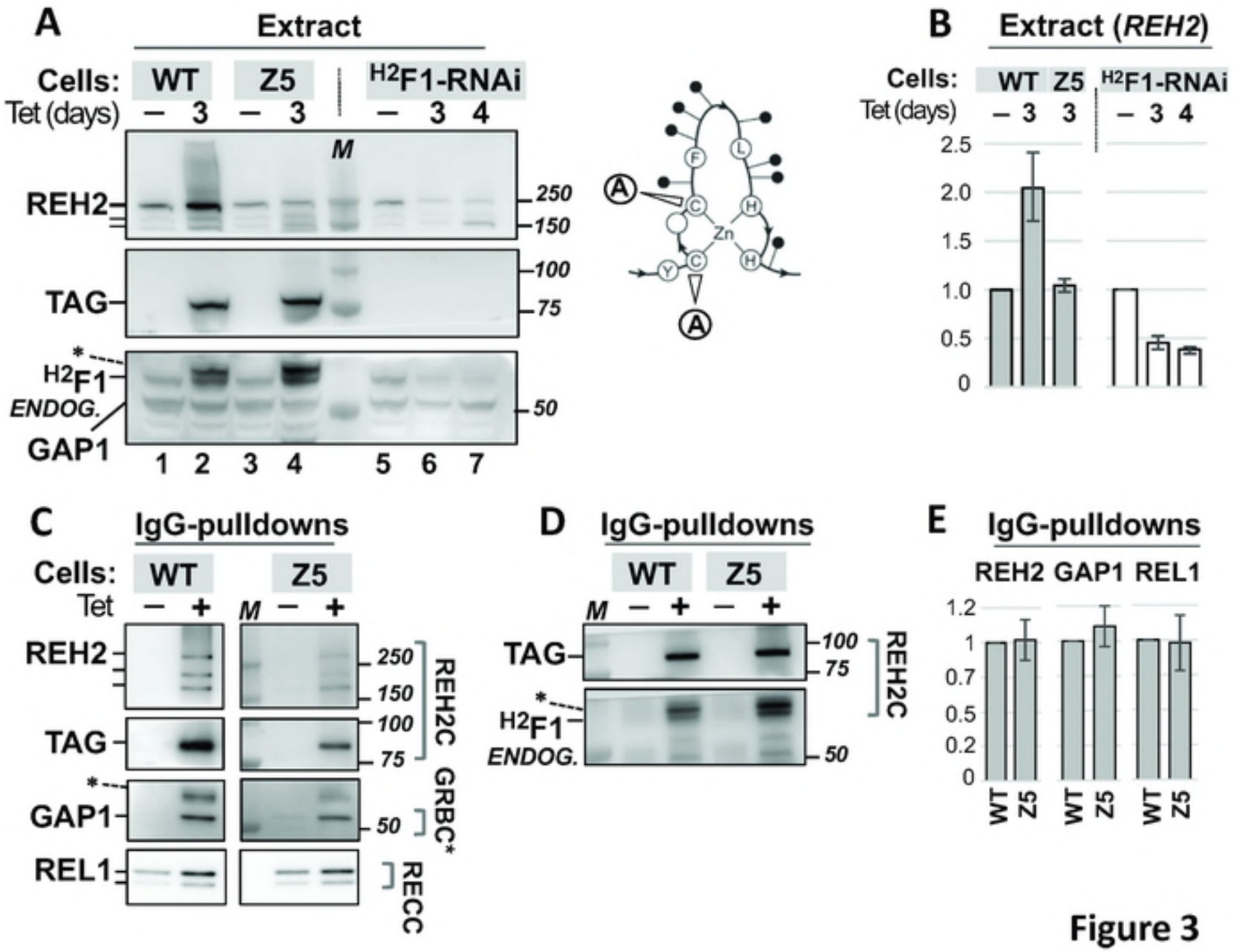

Figure 3

Figure 3

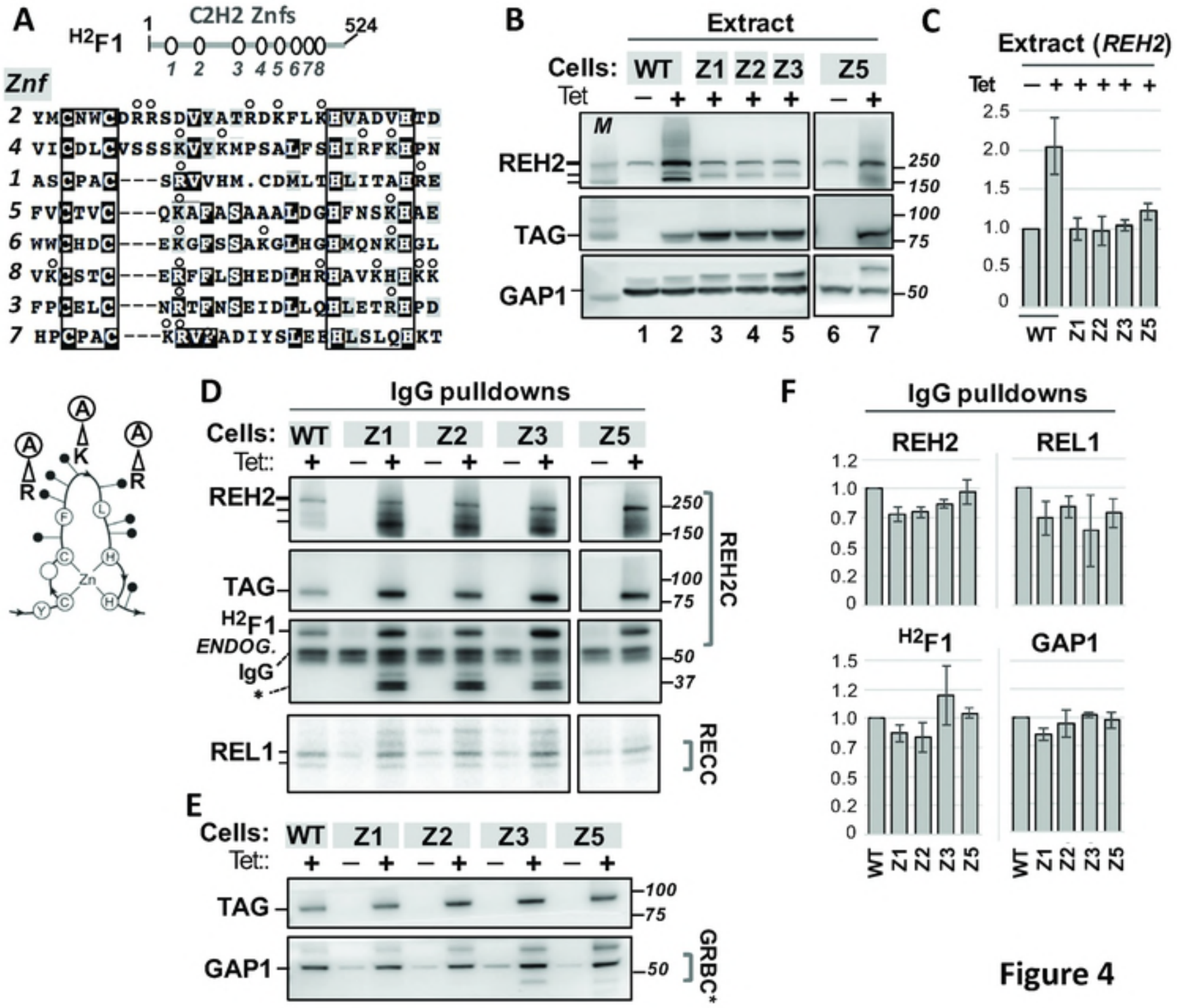
A
H2F1
C2H2 Znfs
1
524
Znf
B
Extract
Cells: WT Z1 Z2 Z3 Z5
Tet
REH2
TAG
GAP1
250
150
100
75
50
1 2 3 4 5 6 7
C
Extract (REH2)
Tet
WT Z1 Z2 Z3 Z5
D
IgG pulldowns
Cells: WT Z1 Z2 Z3 Z5
Tet::
REH2
TAG
H2F1
ENDOG.
IgG
REL1
250
150
100
75
50
37
REH2C
RECC
E
Cells: WT Z1 Z2 Z3 Z5
Tet::
TAG
GAP1
100
75
50
GRBC*
F
IgG pulldowns
REH2
REL1
H2F1
GAP1
WT Z1 Z2 Z3 Z5
Figure 4

Figure 4

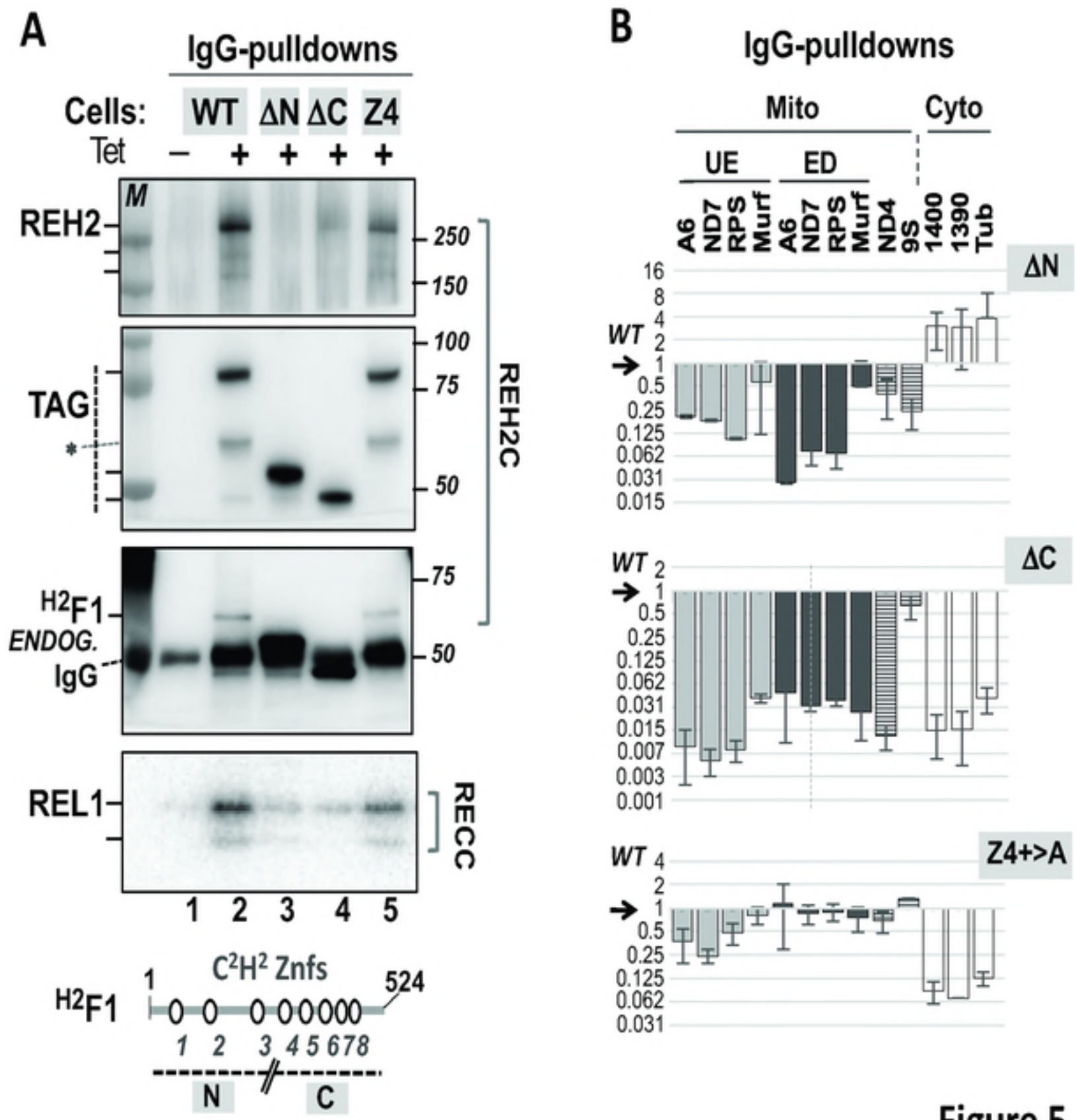

Figure 5

Figure 5

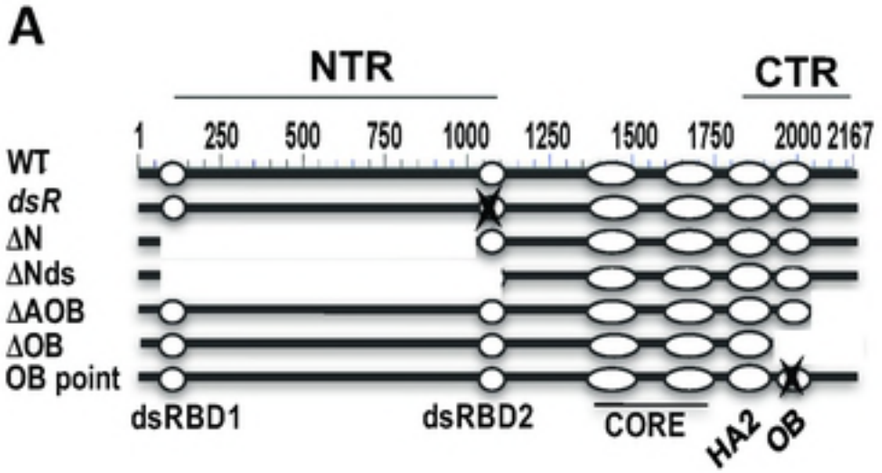

NAME	MUTATION	DOMAINS AFFECTED	MW
dsR	K1078A/A1086D	dsRBD2	242
ΔOB	Δ2045-2167		228
ΔAOB	Δ1908-2167	OB fold	213
ΔN	Δ34-1023	dsRBD1	132
ΔNds	Δ34-1093	dsRBD1/dsRBD2	124
1979	R1979A	OB fold	242
1998	H1998E	OB fold	242
1999	R1999E	OB fold	242
98/99	H1998/R1999	OB fold	242
2023	R2023	OB fold	242

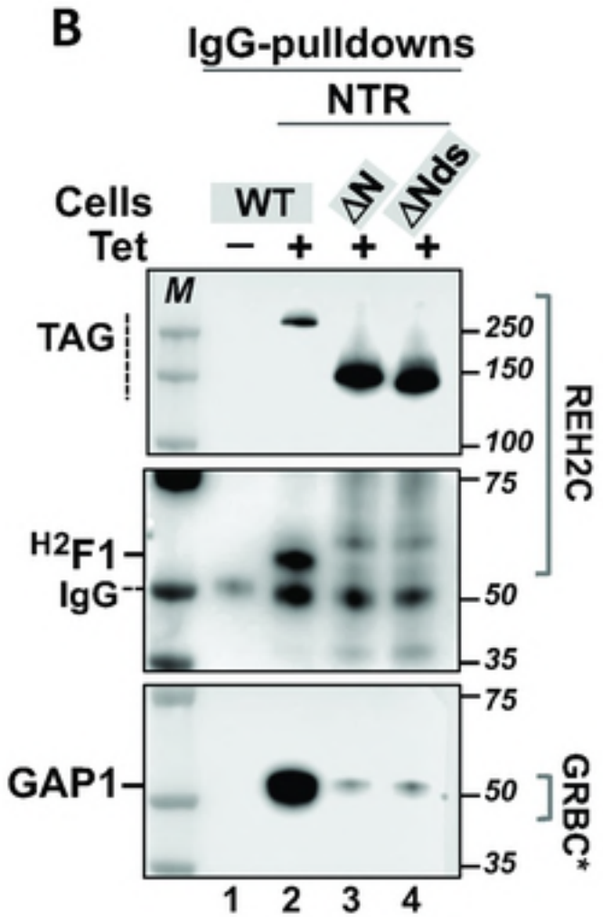

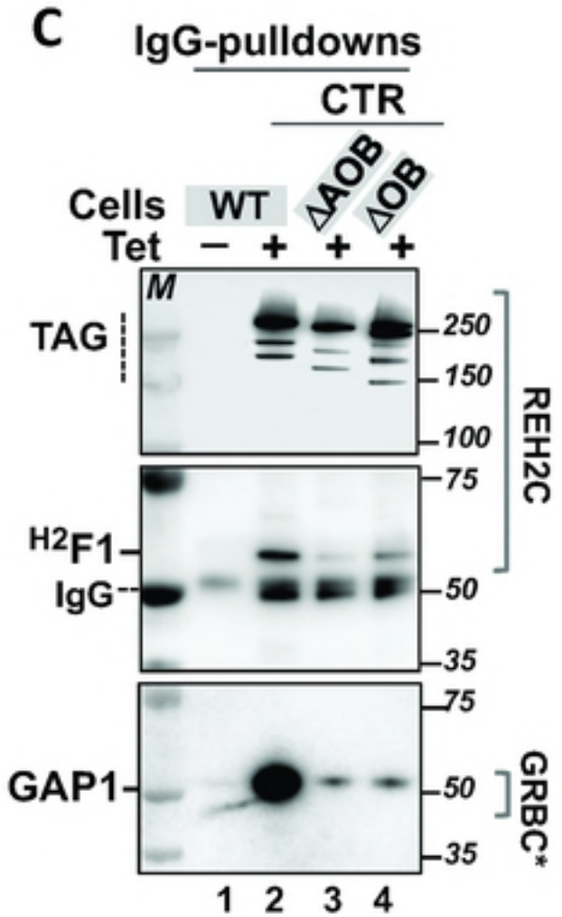

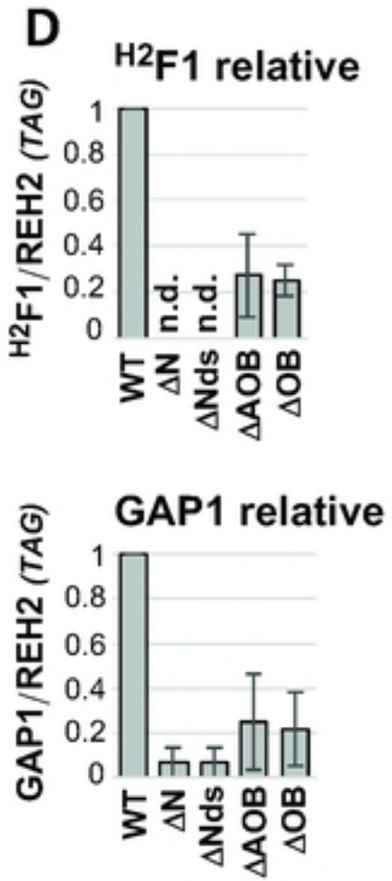

Figure 1

Figure 1

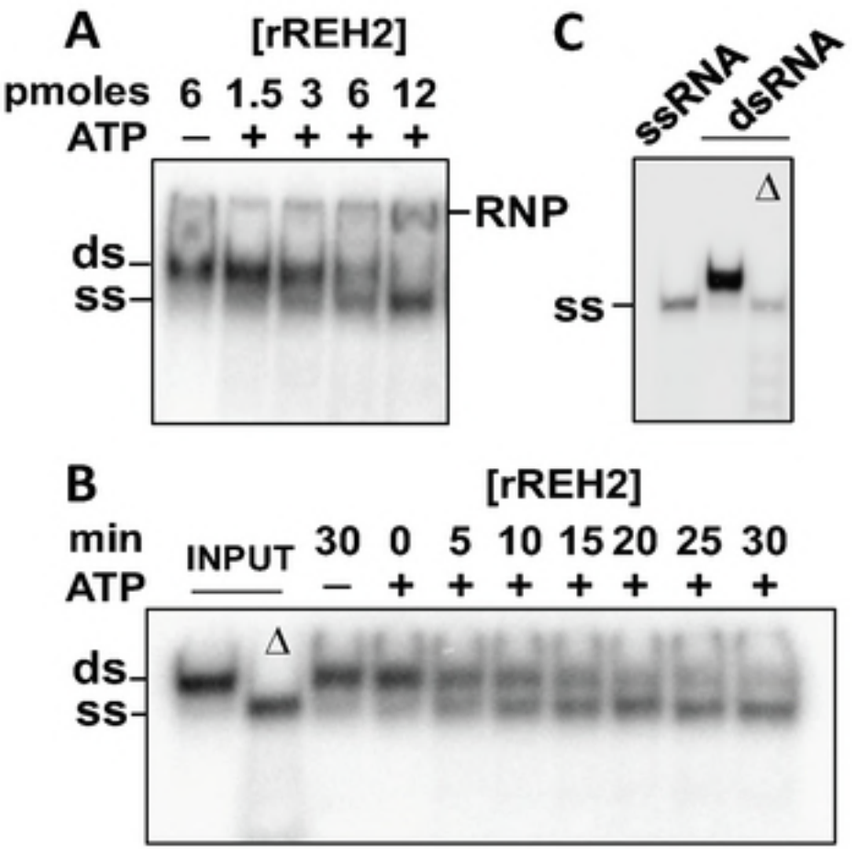

Figure 6

Figure 6